ON THE OSCILLATIONS OF A SEMI-SUBMERSIBLE CATAMARAN HULL AT SHALLOW DRAFT

TAKAKI, Mikio
Research Institute for Applied Mechanics, Kyushu University : Research Associate

ARAKAWA, Hiroyuki
Research Institute for Applied Mechanics, Kyushu University : Research Associate

TASAI, Fukuzo
Research Institute for Applied Mechanics, Kyushu University : Professor

https://doi.org/10.5109/7172194

出版情報：Reports of Research Institute for Applied Mechanics. 19 (64), pp.201-236, 1972. 九州大学応用力学研究所
バージョン：
権利関係：

Reports of Research Institute for Applied Mechanics
Vol.XIX, No. 64, 1972

ON THE OSCILLATIONS OF A SEMI-SUBMERSIBLE CATAMARAN HULL AT SHALLOW DRAFT*

By Mikio TAKAKI,** Hiroyuki ARAKAWA**
and Fukuzō TASAI***

This paper is the second report on the motion of a Semi-Submersible Catamaran Hull (S. S. C. H.) in regular waves and is especially concerned with the motion of S. S. C. H. at shallow draft in head seas and beam seas.

The hydrodynamic coefficients (added mass, damping coefficient etc.) are calculated by using Ohkusu's method, which deals with the calculation of hydrodynamic force and moment working upon multiple cylinders with an arbitrary cross section, and then the equations of the motions of S. S. C. H. in head seas or beam seas can be formulated with the aid of the strip method. The solutions of these equations are good in agreement with the experimental results except for a part of head seas.

The motions of S. S. C. H. theoretically show unique phenomena in short wave periods, which are caused by coupled resonance of rolling and interactions between hydrodynamic forces working upon the caissons.

Usually there are many natural periods in free oscillation of S. S. C. H. theoretically. In the model experiment, however, there appears the only one natural period at the point with the smallest damping force of the theoretical natural periods.

1. Introduction

Recently many types of floating structures for ocean development have been actively built. As these structures have complex forms which are composed of some simple members, the calculation of the hydrodynamic forces acting upon these structures are difficult. Accordingly the evaluations of hydrodynamic forces acting upon these structures have not been made so clearly as those of usual ships.

For the purpose of rational design of these structures, it is necessary to estimate hydrodynamic forces acting upon these structures and investigate the motions of them in waves. The motions of the Semi-Submersible Catamaran

* The paper was read at the Spring Meeting of the Society of Naval Architects of West Japan in Innoshima on May 1971.

** Research Associate, Research Institute for Applied Mechanics, Kyushu University.
*** Professor, Research Institute for Applied Mechanics, Kyushu University.

Hull in full load condition in regular waves were dealt in the first report[1]. In this paper we discuss the motion of a Semi-Submersible Catamaran Hull at ballast condition in regular waves. The hydrodynamic coefficient (added mass, damping coefficient etc.) are calculated by using Ohkusu's method[2], which deals with the calculation of hydrodynamic forces and moments acting upon multiple cylinders with arbitrary cross section. The theoretical calculation by using the **O. S. M.**[3] (Ordinary Strip Method) is compared with the experimental results. The natural frequencies of motions are discussed.

2. Model and Experiments

As shown in Fig. 1, the model of the Semi-Submersible Catamaran Hull (hereafter referred to as **S. S. C. H.**) has two caissons, eight columns and an operation deck on the upper of columns and floats at shallow draft condition. The main particulars of the model are given in Table 1.

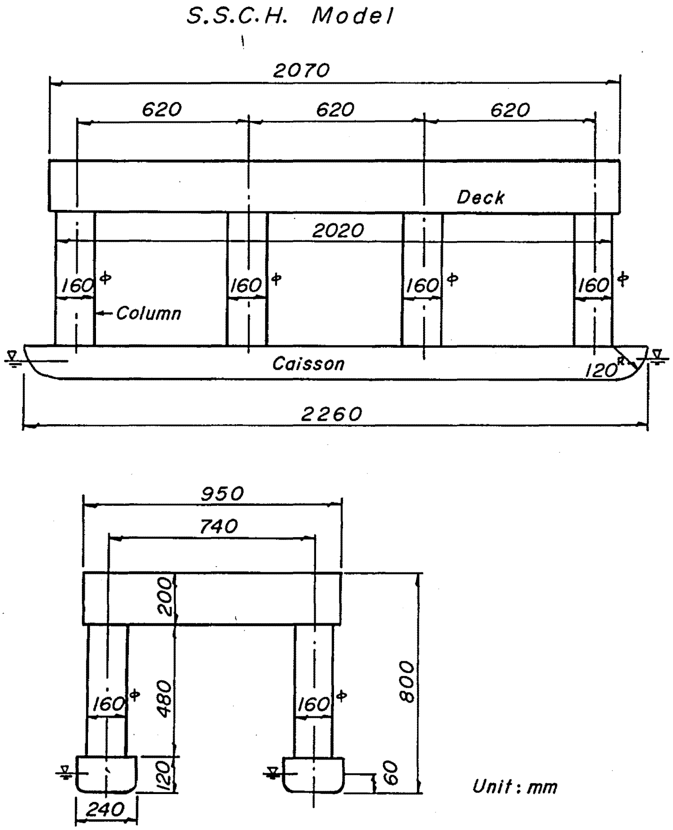

Fig. 1 Semi-Submersible Catamaran Hull Model

Table 1 Particulars of Model

All over length of caisson	$L_{o.a.} = 2.26$ m
Length of water line of caisson	$L_{W.L.} = 2.23$ m
Breadth of caisson	$2b_1 = 0.24$ m
Depth of caisson	$l_1 = 0.12$ m
Distance between caissons	$2b_0 = 0.74$ m
Draft	$T_{\boxtimes} = 0.06$ m
Block coefficient of cross section	$\sigma_{\boxtimes} = 0.9651$
Ratio of half breadth and draft	$H_{0\boxtimes} = b_1/T_{\boxtimes} = 2.0$
Diameter of column	$d = 0.16$ m
Length of column	$h = 0.48$ m
Weight of displacement	$W = 57.76$ kg
Height of center of buoyancy from keel	$KB = 0.03$ m
Height of center of gravity from keel	$KG = 0.133$ m
Transverse metacentric height	$\overline{GM} = 2.433$ m
Longitudinal metacentric height	$\overline{GM_L} = 7.300$ m
Height of center of gravity from surface of still water	$l_G = 0.073$ m
Radius of transverse gyration	$R_\varphi = 0.420$ m
Radius of longitudinal gyration	$R_\theta = 0.622$ m
Natural period of heaving	$T_Z = 0.756$ sec
Natural period of rolling	$T_\varphi = 0.646$ sec
Natural period of pitching	$T_\theta = 0.723$ sec

It is supposed that the dimension of the actual structure is about fifty times as large as that of the model. The model experiment was performed in the experimental tank ($L \times B \times D \times d = 80\text{m} \times 8\text{m} \times 3.5\text{m} \times 3\text{m}$) of the Research Institute for Applied Mechanics of Kyushu University. In the experiment of head sea condition the model was towed with a chain. This chain was about 15m long and had a tension which beared hydrodynamic drag in waves. As show in Fig. 2, the chain was hung down a depth of about 2m under a free surface of still water and a balancing weight was attached at the lowest point of the catenary to prevent the model from drifting to backward due to wave force. Simultaneously a balancing weight was adjusted with a thread to keep the depth of catenary.

In the experiment of beam sea condition the chain was detached and the motions of **S. S. C. H.** were measured at zero advance speed. For measuring the motions of model, a similar instrument to that described in reference (4) was used and this instrument was set at the center of stand between the caissons (the point Q in Fig. 3).

3. Hydrodynamic Forces Working upon the Catamaran Hull

Let us suppose that **S. S. C. H.** has heaving $z=R_e[e^{i\omega t}]$, swaying $y=R_e[e^{i\omega t}]$

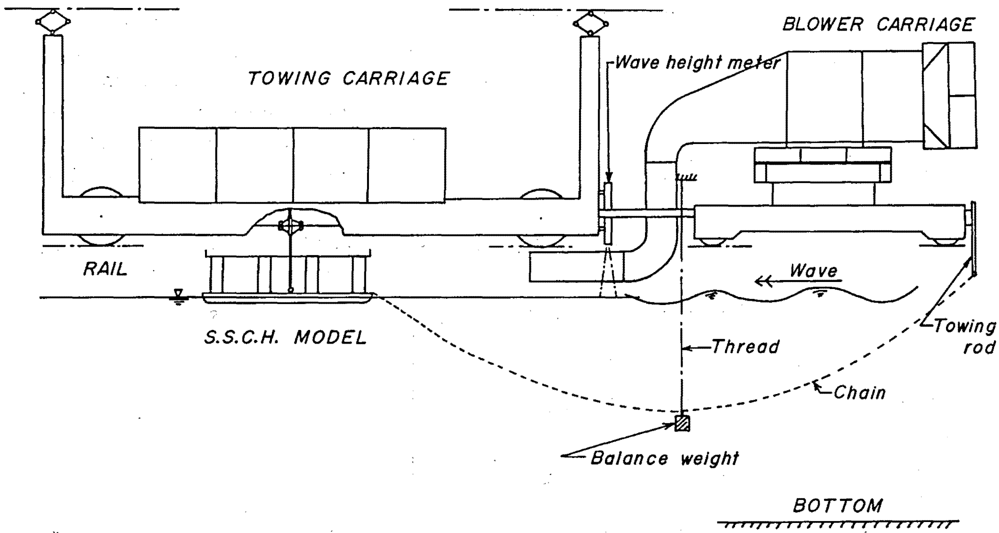

Fig. 2 Schematic arrangement of measuring instruments

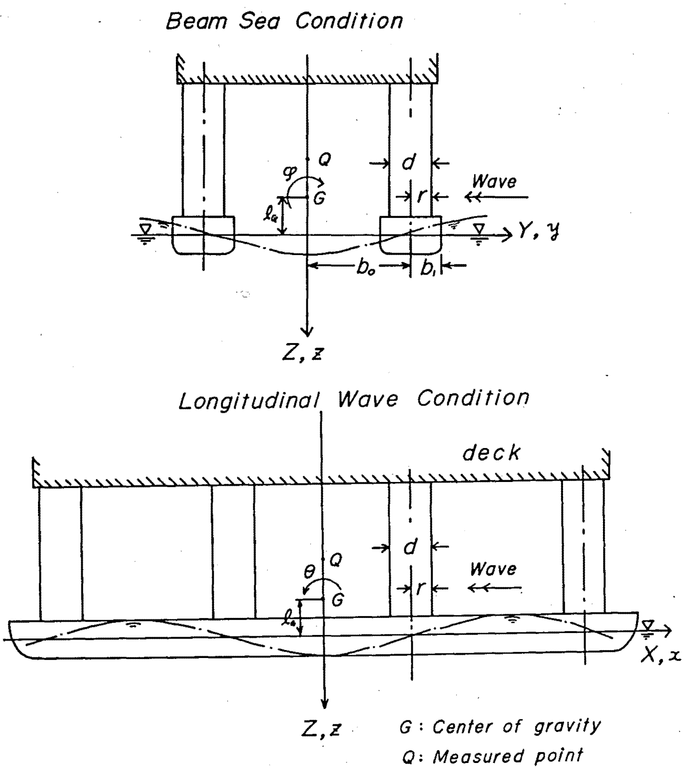

Fig. 3 System of coordinates and regular waves

and rolling $\varphi = R_e[e^{i\omega t}]$ about the origin O on a free surface of still water as shown in Fig. 3.

Taking hydrodynamic interactions working upon the two dimensional caissons into accout by using Ohkusu's method[2], the added mass coefficients (the added mass moment of inertia coefficienst in the case of rolling oscillation), the amplitude ratios of diverging wave at infinity and it's phases are expressed as follows:

Motion	Added mass coefficient	Amplitude ratio of diverging wave	Phase
Heaving	$=\dfrac{\text{Added mass of heaving motion}}{4\rho\sigma bT}$	$\overline{A}_H$	ε_H
Swaying	$=\dfrac{\text{Added mass of swaying motion}}{4\rho\sigma bT}$	$\overline{A}_S$	ε_S
Rolling	$=\dfrac{\text{Added mass moment inertia}}{4\rho\sigma bT^2}$	$\overline{A}_R$	ε_R

where $2b$, T and σ are breadth, draft and block coefficient of cross section respectively. The numerical examples are shown in Fig. 4, 5 and 6.

Thus, as the solutions of radiation problems are known, the hydrodynamic forces and moments per unit length due to regular wave $\zeta_a e^{i(\omega t+KY)}$ can be expressed, using Bessho's theory developed from Haskind-Newman relation, in the following simple formula.

Direction	Force (or moment)	
Y	$\dfrac{i\rho g}{K}\zeta_a \overline{A}_S e^{i(\varepsilon_S+\omega t)}$	(1)
Z	$\dfrac{i\rho g}{K}\zeta_a \overline{A}_H e^{i(\varepsilon_H+\omega t)}$	(2)
Mt. about O	$\dfrac{i\rho g}{K}T\zeta_a \overline{A}_R e^{i(\varepsilon_R+\omega t)}$	(3)

where ρ: water density

g: gravity acceleration

K: wave number $\left(=\dfrac{\omega^2}{g}=\dfrac{2\pi}{\lambda}\right)$

4. Motions in Beam Sea Condition

4. 1. The equation of motions

As shown in Fig. 3, assuming that **S. S. C. H.** is floating at zero advance speed on a still free water surface (XY-plane) and that a regular wave ζ_a progresses to the $-Y$ direction, let us consider about the heaving motion z, the swaying motion y and the rolling motion φ about the center of gravity G.[5),7)]

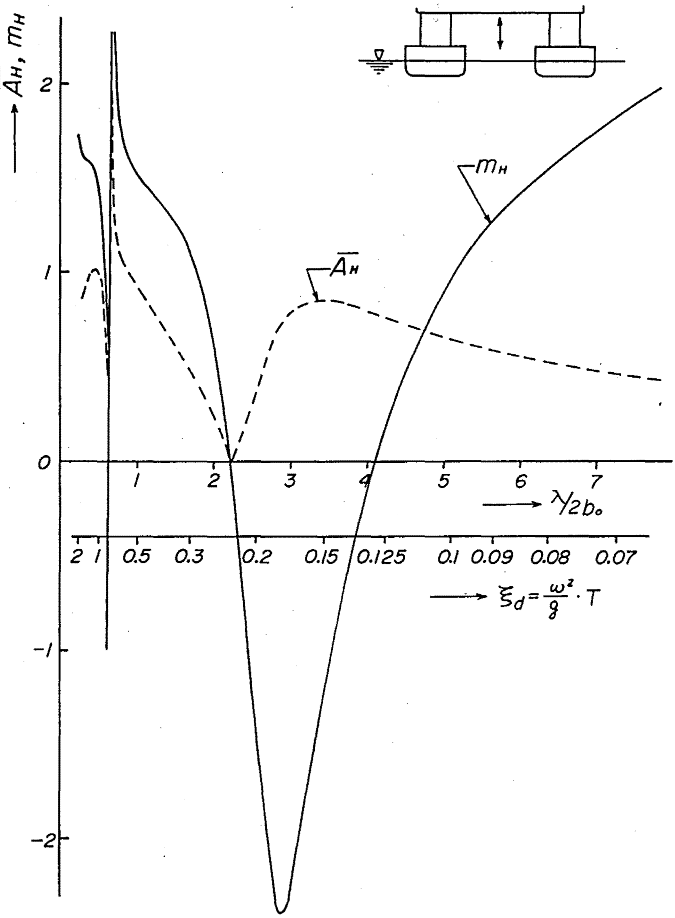

Fig. 4 Wave amplitude $\bar{A}_H$, added mass coefficient m_H for heaving 2-cylinders

Since radiation forces, wave exciting forces and moments acting upon the each cross section are known in the foregoing paragraph, the equations of the heaving, swaying and rolling motions about the center of gravity G are given as follows:

$$a_{11}\ddot{y}+a_{12}\dot{y}+b_{11}\ddot{\varphi}+b_{12}\dot{\varphi}=F_S \tag{4}$$

$$a_{21}\ddot{\varphi}+a_{22}\dot{\varphi}+a_{23}\varphi+b_{21}\ddot{y}+b_{22}\dot{y}=M_t \tag{5}$$

$$a_{31}\ddot{z}+a_{32}\dot{z}+a_{33}z=F_H \tag{6}$$

where

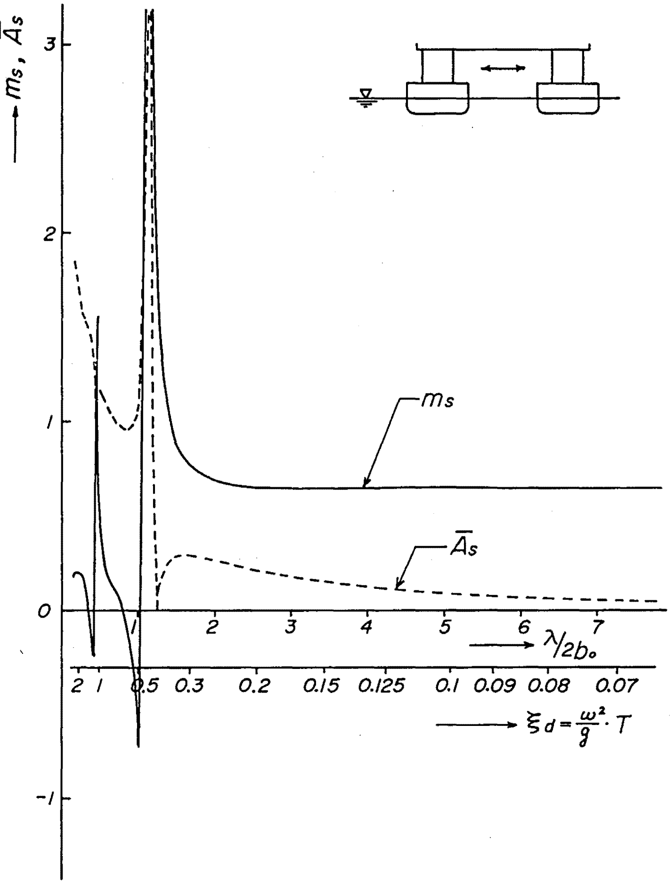

Fig. 5 Wave amplitude $\overline{A}_S$, added mass coefficient m_S for swaying 2-cylinders

$$
\left\{
\begin{aligned}
a_{11} &= \frac{W}{g} + \int_L 4\rho\sigma bTm_S dx, \qquad a_{12} = \int_L \frac{\rho g^2}{\omega^3} \overline{A}_S{}^2 dx, \\
b_{11} &= \int_L 4\rho\sigma bT(m_S l_G + M) dx, \qquad b_{12} = \int_L \frac{\rho g^2}{\omega^3} (\overline{A}_S{}^2 l_G + N) dx, \\
F_S &= \int_L \frac{i\rho g \zeta_a}{K} \overline{A}_S e^{i(\varepsilon_S + wt)} dx, \\
a_{21} &= J_\varphi + \int_L 4\rho\sigma bT(m_S l_G{}^2 + 2M \cdot l_G + m_R) dx, \\
a_{22} &= \int_L \frac{\rho g^2}{\omega^3} (\overline{A}_S{}^2 l_G{}^2 + 2N \cdot l_G + \overline{A}_R{}^2) dx,
\end{aligned}
\right.
$$

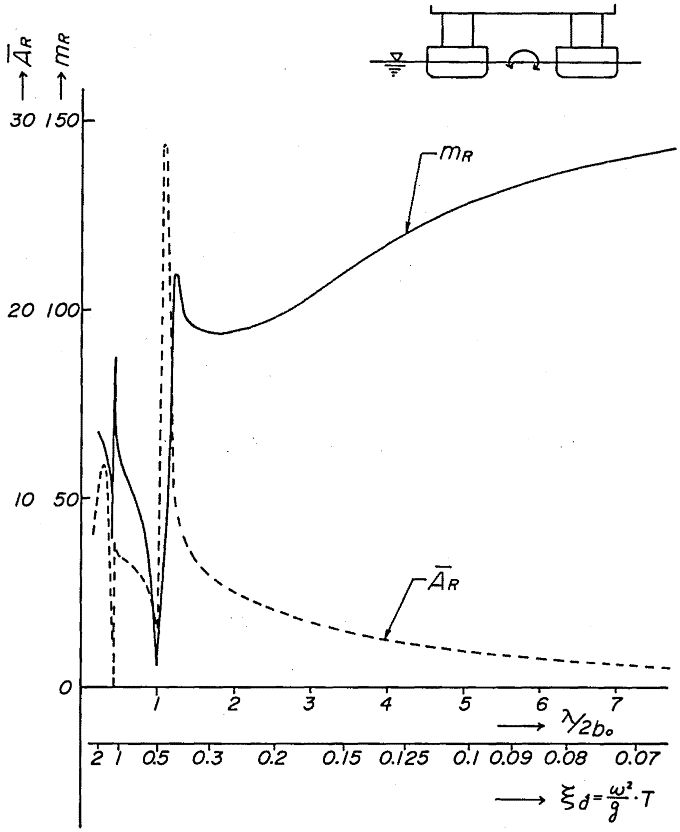

Fig. 6 Wave amplitude $\bar{A}_R$, addedmass moment inertia coefficient m_R for rolling 2-cylinders

$$\left\{\begin{aligned}
&a_{23}=W\cdot\overline{GM}, \qquad b_{21}=b_{11}, \qquad b_{22}=b_{12},\\
&M_t=\int_L \frac{i\rho g\zeta_a}{K}(T\,\overline{A}_R e^{i\varepsilon_R}+l_G\,\overline{A}_S e^{i\varepsilon_S})e^{i\omega t}dx,\\
&a_{31}=\frac{W}{g}+\int_L 4\rho\sigma bTm_H dx,\\
&a_{32}=\int_L \frac{\rho g^2}{\omega^3}\overline{A}_H{}^2 dx, \qquad a_{33}=\rho gA_w,\\
&F_H=\int_L \frac{i\rho g\zeta_a}{K}\overline{A}_H e^{i(\varepsilon_H+\omega t)}dx.
\end{aligned}\right. \tag{7}$$

J_φ: transverse mass moment of inertia about the center of gravity **G**

A_w: area of water plane

M, N: coefficient of rolling moment about origin **O** due to the swaying motion, $M=-m_S \cdot l_{SR}$, $N=-N_S \cdot l_w$.

The free oscillation test of **S. S. C. H.** was made on a free surface of still water and the natural period was measured. Substituting the natural period into the equations, the coupled equations of the free rolling and swaying oscillations were obtained. Thus the transverse mass moment of inertia was obtained (we will discuss the natural period again at later paragraph). The instrument of measuring motion was set at the point Q, $l_0=0.16$m above the origin **O** (Fig. 3). The signs z_a, y_a and φ_a denote the heaving, swaying displacement and rolling angle respectively. Substituting $z=z_a e^{i\omega t}$, $y=y_a e^{i\omega t}$ and $\varphi=\varphi_a e^{i\omega t}$ into the coupled equations (4), (5) and (6), the amplitude and the phase of each motion can be obtained. The numerical results of the amplitudes and the phases of motions are shown in Fig. 7~Fig. 12.

4. 2. Comparison of the experimental results and the calculation results

The amplitudes of the heaving, swaying and rolling motions of the model were measured in beam sea condition. The drift of model due to wave forces in beam sea condition was free and the towing chain was detached from the model. The periods of generated waves were 0.77 sec~1.54 sec ($\lambda/2b_0=1.25$~5.0) and steepness of wave H/λ was constant (1/50). The experimental results are shown with the calculation results in Fig. 7, 8 and 9. As shown in these figures, it can be concluded that theoretical and experimental results are in

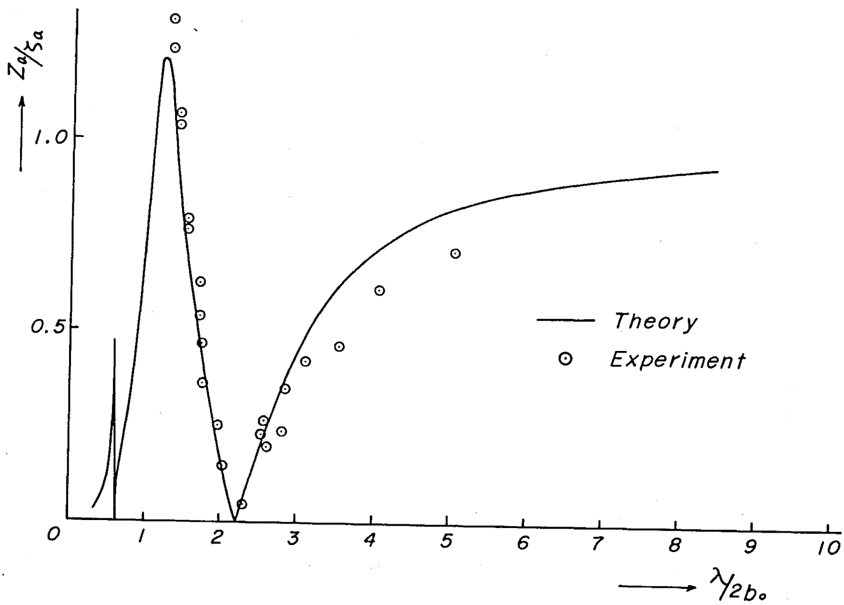

Fig. 7 Heaving motion of S. S. C. H. in beam seas

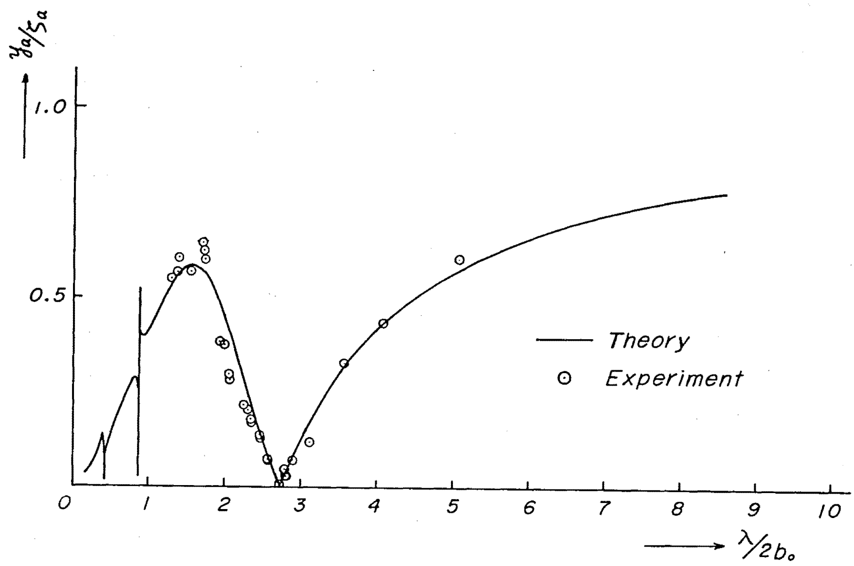

Fig. 8 Swaying motion of S. S. C. H. in beam seas

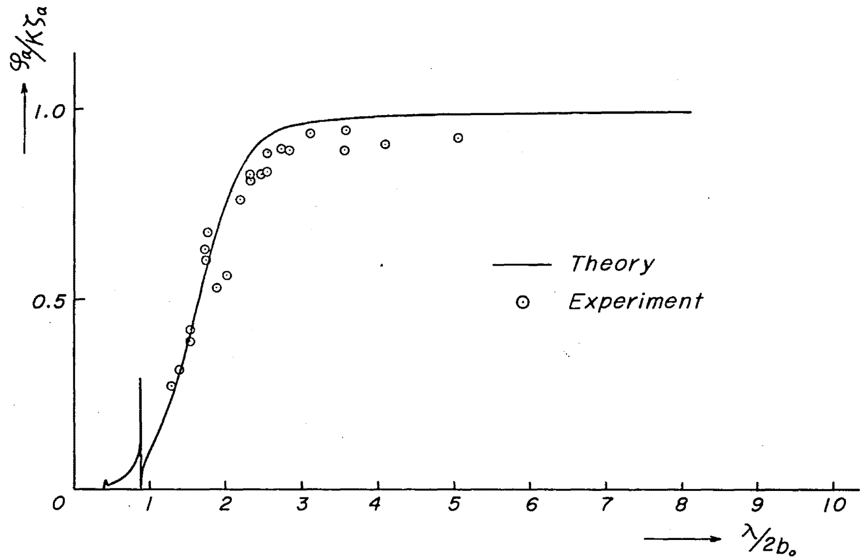

Fig. 9 Rolling motion of S. S. C. H. in beam seas

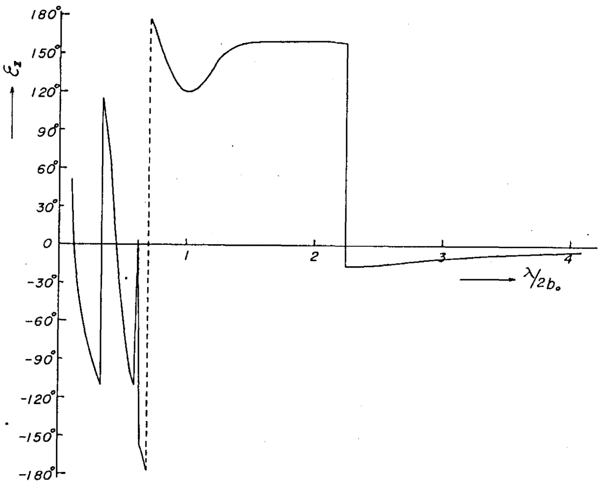

Fig. 10 Heaving phase lag ε_z in beam seas

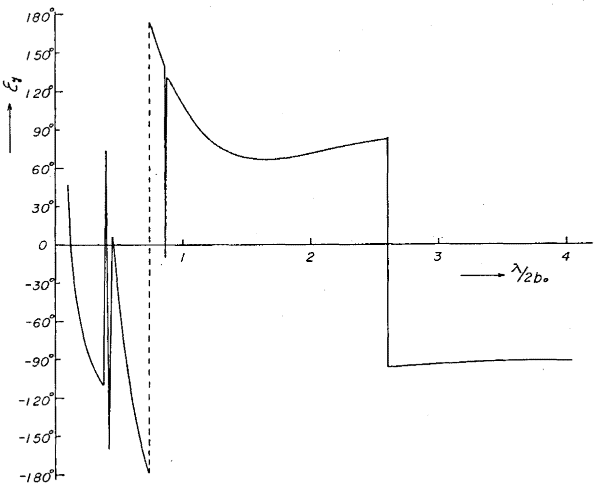

Fig. 11 Swaying phase lag ε_y in beam seas

good agreement. In our experiments and calculations some remarkable phenomena are observed. As shown in Fig. 4, 5 and 6 of the foregoing paragraph, there are a few periods where the amplitudes of waves diverging at infinity are zero. Hereafter we call it waveless point. It is obvious in our numerical results that these waveless points occur in the range of high frequencies. As for the heaving motion it can be seen that the points of zero amplitude coincide with the waveless points in Fig. 4 and 7. As these waveless points do not

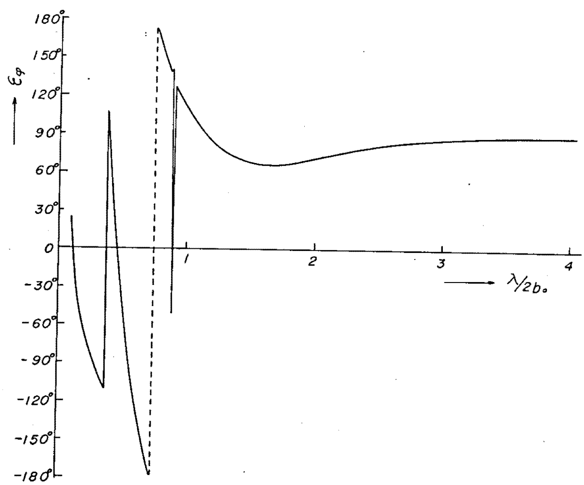

Fig. 12 Rolling phase lag ε_φ in beam seas

coincide with the resonant frequency of heaving motion, it is obvious that the amplitude of heaving motion is equal to zero at these waveless points. These phenomena are shown in our experiments in Fig. 7.

On the contrary, the rolling and swaying motions are not so simple as the heaving motion, because of the hydrodynamic interactions between caissons and the mutual influence of coupled motion, that is, the zero amplitudes of rolling and swaying motion do not occur at waveless points. In the range of high frequency the phases of rolling and swaying motions are almost the same, but in the range of low frequency, i. e., over the period $\lambda/2b_0 \doteqdot 2.6$ the difference of phase angle of rolling and swaying motion is π in Fig. 11 and 12.

The amplitude of swaying motion is equal to zero near $\lambda/2b_0 = 2.75$. That is not due to waveless point but due to the coupling influence of rolling into the swaying motion.

5. Motions in Head Sea Condition

5. 1. The equations of motions

The radiation problems were solved in the section 3, taking hydrodynamic interaction between two dimensional cross section into account. These results are applied to the calculation of motion of **S. S. C. H.** in head sea condition with aid of the **O. S. M.**[3] in order to solve the coupled equations of heaving motions.

The coupled equations of heaving and pitching motions about the center of gravity G are given as follows[3] :

$$\left(\frac{W}{g}+a\right)\ddot{z}+b\dot{z}+cz+d\ddot{\theta}+e\dot{\theta}+g_1\theta=F_c\cos\omega t-F_s\sin\omega t, \tag{8}$$

$$(J_\theta+A)\ddot{\theta}+B\dot{\theta}+C\theta+D\ddot{z}+E\dot{z}+Gz=M_c\cos\omega t-M_s\sin\omega t, \tag{9}$$

where

$$\left\{\begin{aligned}
a &= \int_L 4\rho\sigma bTm_H dx,\\
b &= \int_L \frac{\rho g^2}{\omega^3}\overline{A_H}^2 dx,\\
c &= \rho gA\omega,\\
d &= -\int_L 4\rho\sigma bTm_H x dx,\\
e &= -\int_L \left(\frac{\rho g^2}{\omega^3}\overline{A_H}^2 x-4\rho\sigma bTm_H V\right)dx,\\
g_1 &= -\int (4\rho gbx-\frac{\rho g^2}{\omega^3}\overline{A_H}^2 V)dx,\\
F_c &= \zeta_a\int_L [(4\rho gb-\omega\omega_e 4\rho\sigma bTm_H)exp(-KT_m)\cos Kx\\
&\qquad -\omega\exp(-KT_m)\frac{\rho g^2}{\omega^3}\overline{A_H}^2\sin Kx]dx,\\
F_S &= \zeta_a\int_L [4\rho gb-\omega\omega_e 4\rho\sigma bTm_H)\exp(-KT_m)\sin Kx\\
&\qquad +\omega\exp(-KT_m)\frac{\rho g^2}{\omega^3}\overline{A_H}^2\cos Kx]dx,\\
A &= \int_L 4\rho\sigma bTm_H x^2 dx,\\
B &= \int_L \frac{\rho g^2}{\omega^3}\overline{A_H}^2 x^2 dx,\\
C &= -\int_L 4\rho\sigma bTm_H V^2 dx+\rho gI_w,\\
D &= -\int_L 4\rho\sigma bTm_H x dx,\\
E &= -\int_L \frac{\rho g^2}{\omega^3}\overline{A_H}^2 x+4\rho\sigma bTm_H V)dx,\\
G &= -\int_L 4\rho gbx dx,
\end{aligned}\right.$$

$$\left\{\begin{aligned} M_c &= \zeta_a \int_L \Big[\Big(\frac{\rho g^2}{\omega^2}\overline{A_H}^2 x + 4\rho\sigma bTm_H\omega V\Big)exp(-KT_m)\sin\, Kx \\ &\qquad -(4\rho gbx - 4\rho\sigma bT\omega\omega_e m_H x)exp(-KT_m)\cos\, Kxdx, \\ M_S &= \zeta_a \int_L \Big[-\Big(\frac{\rho g^2}{\omega^2}\overline{A_H}^2 x + 4\rho\sigma bTm_H\omega V\Big)exp(-KT_m)\cos Kx \\ &\qquad -(4\rho gbx - 4\rho\sigma bT\omega\omega_e m_H x)exp(-KT_m)\sin Kx\Big]dx. \end{aligned}\right. \tag{10}$$

J_θ : londitudinal mass moment of inertia

I_w : londitudinal moment of water plane area

$\omega_e = \omega + KV$, ω : wave frequency

V : ship advance speed.

The amplitudes of heaving and pitching motions at $F_n=0$, 0.05 and 0.10 are calculated and shown in Fig. 13 and 14, and the phases of these motions are shown in Fig. 15 and 16. The curves which have been obtained by the equations without interaction between caissons are represented by dotted line in Fig. 13 and 14.

5. 2. Comparison of the expertmental results and the calculation results

The amplitudes of heaving and pitching motions were measured in regular head waves. Wave steepness H/λ was constant (1/50) in the same way as in beam sea condition. As shown in Fig. 2 the model was towed with a chain in head waves. And a weight was hung at the lowest position of the catenary to balance with drag force. The amplitudes of heaving and pitching motions in head sea condition are shown in Fig. 13 and 14. As seen from these figures it can be concluded that the theoretical and the experimental results are in good agreement except for the amplitude of heaving motion in the range of wave periods $\lambda/L=0.7\sim0.8$ at $F_n=0$. It was found in our experiments that the chain was oscillating violently in the range of these wave periods. Accordingly we infered from the condition of chain oscillating that the above differences of the theoretical and the experimental results are due to the influence of oscillating motion of chain.

As for the theoretical calculation, it can be seen in Fig. 13 and 14 that the effect of the hydrodynamic interaction between two caissons is small. On the contrary, when the distance two caissons is small, the hydrodrodynamic interaction becomes large[7]. We would like to investigate the effect towing speed on hydrodynamic interaction and the coupling effect of the chain into the oscillation of model etc. in the future.

6. Free Oscillation

For precise prediction of the motion of structures in waves it is very important to know the natural period of floating structures. In this section the

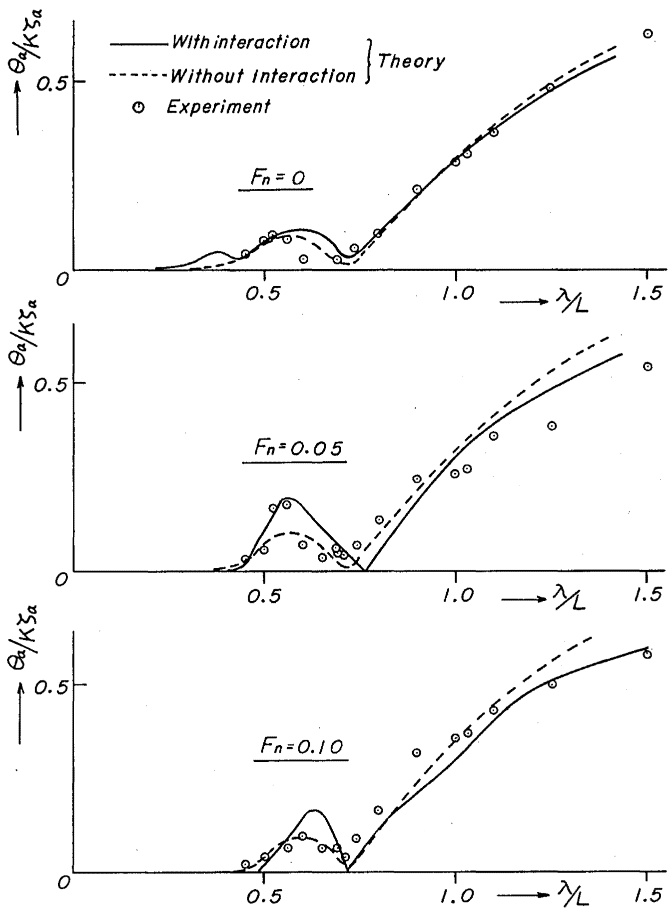

Fig. 13 Pitching motion of S. S. C. H. in head seas

natural periods of heaving and rolling motions of the model are theoretically calculated and the above computed values are compared with the experimental result obtained in the free oscillation. And it is discussed how the values of natural periods affect the motions of structure in waves.

6. 1. The approximate calculation of uatural period

The equations of the free heaving and rolling of structure floating on a free surface in still water are given as follows:

$$(m+\Delta m)\ddot{z}+N\dot{z}_H+\rho g A_w z=0 \tag{11}$$

$$(J_\varphi+I_\varphi)\ddot{\varphi}+N_\varphi\dot{\varphi}+W\cdot\overline{GM}\varphi=0. \tag{12}$$

Now neglecting the damping terms and substituting $z=z_a e^{i\omega t}$ and $\varphi=\varphi_a e^{i\omega t}$ into

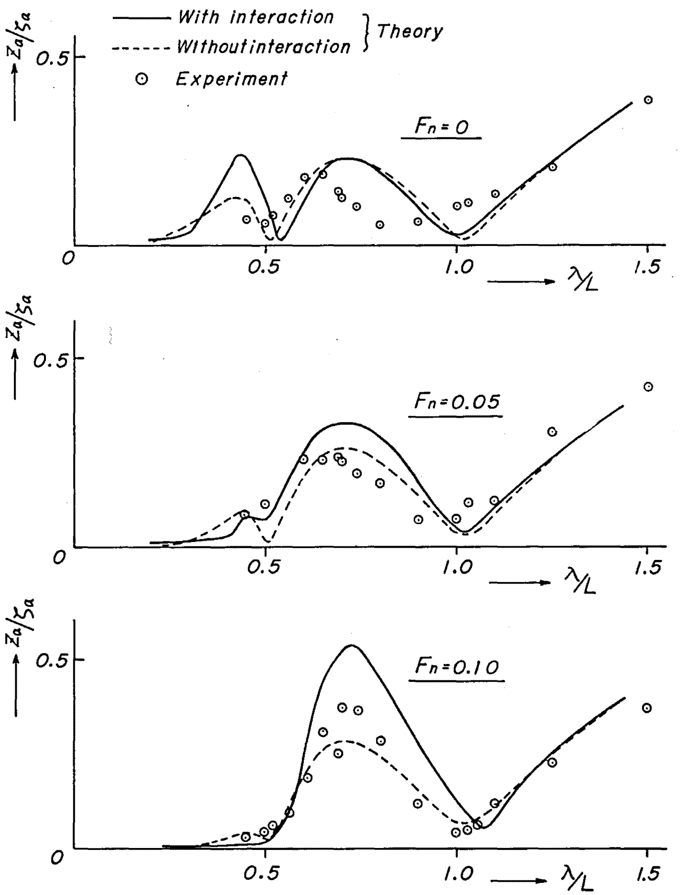

Fig. 14 Heaving motion of S. S. C. H. in head seas

the above equations, we obtain following equations:

$$-\omega^2(m+\Delta m)+\rho g A_w=0 \tag{13}$$

$$-\omega^2(J_\varphi+I_\varphi)+W\cdot\overline{GM}=0. \tag{14}$$

Since Δm and I_φ are the function of circular frequency ω, we put

$$f_H(\omega)=-\omega^2(m+\Delta m)+\rho g A_w \tag{15}$$

$$f_R(\omega)=-\omega^2(J_\varphi+I_\varphi)+W\cdot\overline{GM}. \tag{16}$$

Using the equation (15) and (16), the values of $f_H(\omega)$ and $f_R(\omega)$ which are shown in Fig. 17 are calculated. The circular frequencies ω at $f_H(\omega)=0$ and $f_R(\omega)=0$ are obtained from the above results. These ω are approximately equal to the natural frequencies of heaving and rolling oscillations. The comparison

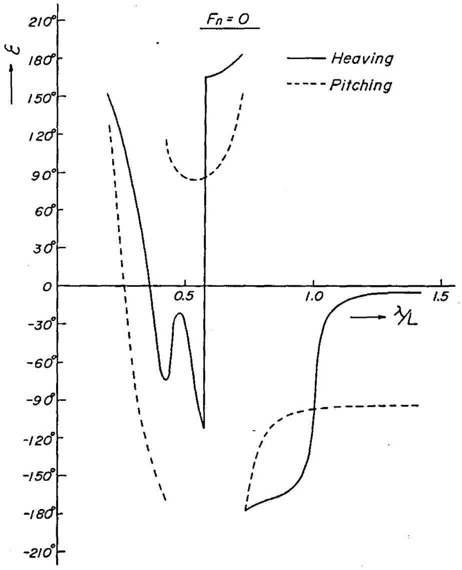

Fig. 15 Phase lag in head seas ($Fn=0$)

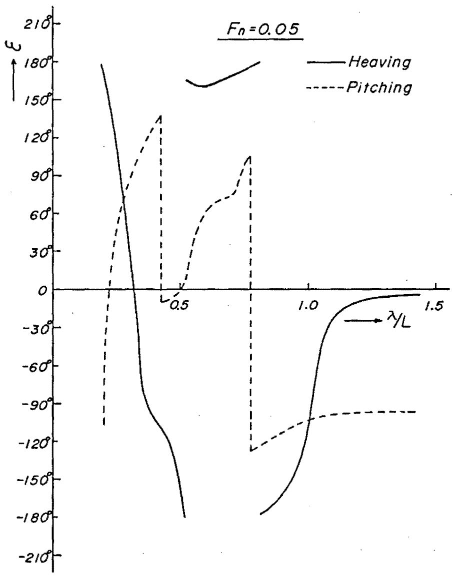

Fig. 16 Phase lag in head seas ($Fn=0.05$)

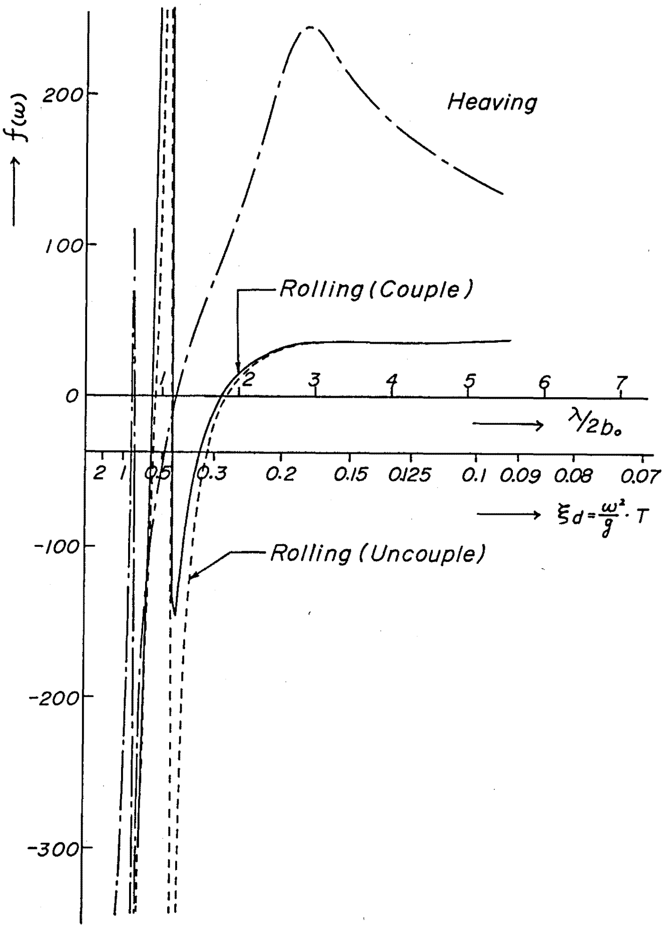

Fig. 17 Natural periods

of computed values and experimental results are given in Table 2.

As shown in Table 2, theoretically three natural periods are obtained in

Table 2 Natural period of uncoupled oscillation

	Heaving Oscillation			Rolling Oscillation		
	T_Z(sec)	ω_Z(1/sec)	ξ_d	T_φ(sec)	ω_φ(1/sec)	ξ_d
Experiment	0.756	8.331	0.423	0.646	9.725	0.579
Theory	0.534	11.777	0.849	0.657	9.563	0.560
	0.551	11.403	0.796	0.731	8.601	0.453
	0.742	8.470	0.439	0.934	6.727	0.277

free heaving and rolling oscillations respectively. On the contrary, in our experiments the only one natural period is respectively obtained. One of three calculated natual periods is nearly equal to the experimental one and the other two differ largely from the experimental result. Accordingly there theoretically exist many natural periods in free oscillation of **S. S. C. H.** which has large hydrodynamic interactions between the two caissons. In the model experiments there appeared the only one natural period, where the damping force is the smallest. As seen from above results, there are natural periods which do not appear in the experiments, but can be obtained by theoretical calculation. Hereafter we call these periods sub-natural periods. The peak of heaving motion at $\lambda/2b_0=0.6$ in Fig. 7 is due to the resonance at the sub-natural period.

In Fig. 7 the curve of swaying amplitude has a sharp peak near the natural period of rolling ($\lambda/2b_0=0.88$, in our experiment). The swaying motion of a system with one degree of freedom doesn't have a natural period and there cannot exist the resonance in waves. But when the swaying motion is affected by the coupling action of rolling, there appears the natual period. Then if the damping forces of swaying and rolling motion are small, the amplitude of swaying motion in waves becomes large. The coupled equations of rolling and swaying motions in beam sea condition are calculated neglecting the viscous damping force. The amplitude of swaying motion is shown in Fig. 18. The coupling effect of rolling into the swaying motion increases near the natural period of rolling motion and a large peak of resonance comes out. One of the

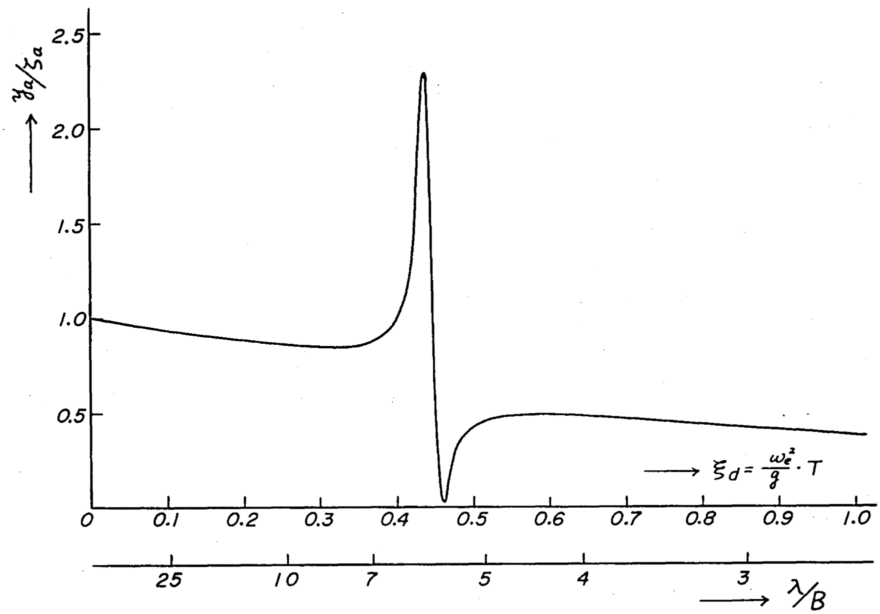

Fig. 18 Swaying motion of 1-cylinder in beam seas

authors has called it **"Coupled Resonance"**, and discussed in detail in his paper[8]. The peak of swaying amplitude at $\lambda/2b_0=0.88$ in Fig. 8 is due to the **Coupled Resonance.**

6. 2. Coupled Oscillation

There are always the coupling effect of swaying motion into the rolling motion. Dr. Ueno discussed the coupling action between swaying and rolling motion[9]. Now we will further solve the coupled equations of free rolling and swaying motion, and obtain the natural period of rolling motion. According to the equation (5) and (6), the coupled equations of free rolling and swaying are approximately obtained as follows:

$$\left.\begin{aligned} &a_{11}\ddot{y}+a_{12}\dot{y}+b_{11}\ddot{\varphi}+b_{12}\dot{\varphi}=0,\\ &a_{21}\ddot{\varphi}+a_{22}\dot{\varphi}+a_{23}\varphi+b_{11}\ddot{y}+b_{12}\dot{y}=0. \end{aligned}\right\} \tag{17}$$

Assuming that effect of damping force is small enough to neglect, the natural circular frequency is obtained by the following equations:

$$\left.\begin{aligned} &a_{11}\ddot{y}+b_{11}\ddot{\varphi}=0,\\ &a_{21}\ddot{\varphi}+a_{23}\varphi+b_{11}\ddot{y}=0. \end{aligned}\right\} \tag{18}$$

Since both y and φ oscillate with circular frequenncy ω, the coupled equations are rewritten as follows:

$$\left.\begin{aligned} &-\omega^2 a_{11}y-\omega\ b_{11}\varphi=0,\\ &-\omega^2 b_{11}y+(-\omega^2 a_{21}+a_{23})\varphi=0. \end{aligned}\right\} \tag{19}$$

Eliminating y from the above equations, ω_n of the natural circular frequency of coupled oscillation is obtained by solving the following equation:

$$-\omega^2 a_{21}+a_{23}+\frac{\omega^2 b_{11}{}^2}{a_{11}}=0. \tag{20}$$

We put

$$F(\omega)=f_R(\omega)+\frac{\omega^2 b_{11}{}^2}{a_{11}}=0, \tag{21}$$

where

$$f_R(\omega)=-\omega^2 a_{21}+a_{23}.$$

The natural frequency of rolling oscillation without the coupling effect of swaying can be obtained by the equation $f_R(\omega)=0$ as mentioned before. Then the comparison of the calculation results and the experimental ones are given in Table 3.

In this condition of the model the difference of the natural rolling period T_φ of a system with one degree of freedom and the natural rolling period T_n

Table 3 Natural period of coupled oscillation

	Rolling Oscillation			
	T_n (sec)	ω_n (1/sec)	ω_n^2/g. T	$\lambda/2b_0$
Experiment	0.646	9.727	0.579	0.88
Theory (Coupe)	0.646*	9.725	0.579	0.88
	0.733	8.572	0.450	1.14
	0.916	6.857	0.288	1.77
Theory (Uncouple)	0.657	9.563	0.560	0.91
	0.731	8.601	0.453	1.12
	0.934	6.727	0.277	1.84

* Since we used the equation (21) to obtain $(J_\varphi+I_\varphi)$ by the experimental results, it was a matter of course that the calculation results agreed with the experimental ones.

as to the coupled oscillation is about 2 percents as shown in Table 3. From the equation (21), the natural circular frequency ω_n is given by the following equation:

$$\omega_n{}^2=\frac{a_{23}}{a_{21}-\dfrac{b_{11}{}^2}{a_{11}}}=\frac{W\cdot\overline{GM}}{(J_\varphi+I_\varphi)-\dfrac{\{m_0m_S(l_G-l_{SR})\}^2}{m_0(1+m_S)}}. \qquad (22)$$

Putting

$$\gamma=\frac{\{m_0m_S(l_G-l_{SR})\}^2}{m_0(1+m_S)}=m_0(l_G-l_{SR})^2\frac{m_S{}^2}{1+m_S}, \qquad (23)$$

the value of γ becomes infinitely large in the case of $m_S=-1$. Then if the value of m_S is nearly equal to -1, the difference of $\omega_\varphi=\sqrt{\dfrac{W\cdot\overline{GM}}{(J_\varphi+I_\varphi)}}$ and ω_n becomes extremely large. From above discussion, it can be concluded that both the free oscillation and the forced oscillation should be dealt with as the coupled oscillation of rolling and swaying motions and that the swaying motion has a peak of resonance due to the coupling effect of rolling motion in the forced oscillations.

7. Conclusion

In order to know the motions of the floating structures in waves, such investions were made as already discussed in this paper. The hydrodynamic coefficient (added mass, damping coefficient etc.) were calculated by using Ohkusu's method, and the motions of **S. S. C. H.** in head sea condition and beam sea condition by using the above values. The calculation results were compared with the experimental results.

In addition, the natural periods of floating structures were theoretically predicted and the above values were compared with the experimental values.

These investigations may be reduced to the following conclusions.

1) The comparison of the calculation and the experimental results is in good agreement in beam sea condition.
2) The agreement between the computational and experimental result in head sea condition is not so good as in beam sea condition, but it is generally good except for a part of them.
3) There are theoretically many natural periods in free oscillation of structure which has much hydrodynamic interaction between the cylinders such as **S. S. C. H.**. In the model experiment, however, there appears the only one natural period at the point with the smallest damping force of the theoretical natural periods.
4) The swaying oscillation has no natural period originally, but the amplitude of swaying motion has a resonant peak in waves due to the coupled effect of rolling motion.

Further investigations would be listed as follows:

a) The speed effect upon a interference of multiple structure.
b) The coupling effect of the towing chain and the floating structure.
c) The transition stage of free oscillation.

Acknowledgements

The authors wish to thank Lecturer M. Ohkusu of Kyushu University for his advice and helpful discussion in this work. We also are indebted to the members of the experimental tank of our institute Kyushu University for their generous assistacnes.

The computing was performed by means of the FACOM 230-60 of the Computer Center of Kyushu University.

References

1) Tasai, F., Nemoto, K., Arakawa, H. and Kurihara, M., A Study on the Motions of a Semi-Submersible Catamaran Hull in Regular Waves, J. S. N. A. of West Japan, No. 40, July, 1970.
2) Ohkusu, M., On the Motion of Multihull Ships in Waves, J. S. N. A. of West Japan, No. 40, July, 1970.
3) Tasai, F. and Takaki, M., Theory and Calculation of Ship Responses in Regular Waves, Symposium on the Seakeeping Quality, S. N. A. of Japan, July, 1969.
4) Tasai, F., Kaname, M. and Arakawa, H., Eqipment for Measuring Six Motions of Ship Model, Rep. Res. Inst. Appl. Mech., Vo.l XIII, No. 45, 1965.
5) Tasai, F., Ship Motions in Beam Seas, Rep. Res. Inst. Appl. Mech., Vol. XIII, No. 45, 1965.
6) Bessho, M., On the Theory of Rolling Motion of Ships among Waves, Report of

Scientific Research of Defence Academy, Vol. 3, No. 1, 1965.
7) Ohkusu, M. and Takaki, M., On the Motion of Multihull Ship in Waves (II), J. S. N. A. of Japan, Vol. 129, June, 1971.
8) Tasai, F., On the Sway, Yaw and Roll Motions of a Ship in Short Crested Waves, J. S. N. A. of West Japan, No. 42, May, 1971.
9) Ueno, K., Theory of Free Rolling of Ships, Memoirs of the Faculty of Engineering, Kyushu Imperial University, Vol. 9, 1942.

(Received September 20, 1971)

Reports of Research Institute for Applied Mechanics
Vol. XIX, No. 64, 1972

GALLOPING AND VORTEX EXCITATION OF A RECTANGULAR BLOCK

By Yasuharu NAKAMURA*) and Taketo MIZOTA**)

Galloping and vortex excitation were experimentally investigated in a wind tunnel on a rectangular block of a side ratio 2 : 1 which was free to oscillate transversely in a uniform flow. The mean angle of attack of the model was varied from zero to 90 deg. The limit-cycle amplitude of model oscillation and the aerodynamic damping coefficient of unsteady lift force were obtained by a free oscillation technique. Discussions were made on the validity of the quasi-steady aerodynamic theory for galloping and on the effects of the wake vortices on the flutter characteristics.

Notations

C_L	Aerodynamic lift coefficient based on 2h
C_D	Aerodynamic drag coefficient based on 2h
C_M	Aerodynamic moment coefficient based on 2h
f	Frequency of oscillation
f_0	Still-air frequency of oscillation
h	Shorter side of rectangular section
k_a	Aerodynamic damping coefficient of unsteady lift force $\left(=\frac{2M}{\rho h^2}\delta_a\right)$
M	Mass of the model per unit length
R	Reynolds number based on h
S	Strouhal number
V	Wind velocity
$\overline{V}$	Reduced velocity $\left(=\frac{V}{fh}\right)$
$\overline{V}_{cr}$	Critical reduced velocity $\left(=\frac{1}{S}\right)$
y	Amplitude of model transverse displacement
α	Mean angle of attack

*) Professor, Research Institute for Applied Mechanics, Kyushu University.
**) Research Associate, Research Institute for Applied Mechanics, Kyushu University.

δ_0 Structural decrement
δ_a Aerodynamic decrement
η Non-dimensional amplitude $\left(=\frac{y}{h}\right)$
η_L Non-dimensional limit-cycle amplitude
ρ Air density

1. Introduction

The recent trends to higher and more slender structures, together with greater refinement of structural design and method of construction tend to increase the susceptibility to aeroelastic instabilities of structures, namely, flutter, when they are exposed to a strong wind. No complete theory of the instabilities is available, because there is no complete aerodynamic theory for any separated flow, particularly a nonsteady one.

Transverse galloping and vortex excitation which will be treated in this paper are most fundamental among various instabilities. The quasi-steady aerodynamic theory for transverse galloping was proposed by Den Hartog[1], where the aerodynamic forces acting on an oscillating structure are determined by using measured stationary aerodynamic force coefficients. Parkinson[2] applied this theory to several bluff sections, where the motion was assumed to be governed by a non-linear differential equation with a small damping. His results showed good agreement between theory and experiment for the square section, but for some other sections including the rectangular one showed rather poor agreement.

Generally speaking, the assumption that the flow around an oscillating structure is equivalent to the steady flow corresponding to the effective angle of attack would restrict the range for which the quasi-steady theory is valid. One can expect good agreement between theory and experiment at high reduced velocities, but not always at low reduced velocities. This is because of the predominant effects of the flow unsteadiness at low reduced velocities.

The other instability, the vortex excitation usually occurs at low reduced velocities, which makes the situation more complicated. It will be difficult to separate galloping and vortex excitation at low reduced velocities when both are possible to occur.

This paper describes the results of a wind tunnel experiment on flutter of a rectangular block of a side ratio 2: 1 which was free to oscillate transversely in a uniform flow. Although the model was a simple one, the purpose of the present experiment was to throw some light on the aeroelastic instabilities of real high-rise buildings. The experiment was conducted for a wide range of mean angle of attack from zero to 90 deg. Discussions were made on the validity of the quasi-steady aerodynamic theory for galloping and on the effects of the wake vortices on the flutter characteristics.

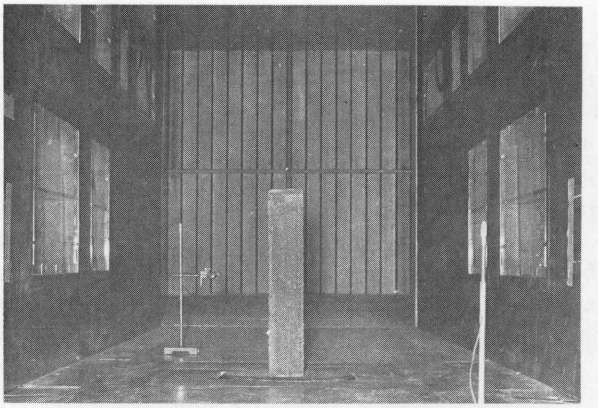

Photo 1 Model rectangular block installed in the test section

(*Facing p.* 226)

2. Wind Tunnel and Model

The 4m × 2m Low-Speed Wind Tunnel at the Research Institute for Applied Mechanics, Kyushu University was used for the present experiment. This tunnel has two interchangeable test sections, one having dimensions of 2m (height) × 4m (width) × 6m (length) and the other, 4m × 2m × 6m; the contraction and the diffuser can be turned by 90 deg about the centre axis. Both of the two test sections were used in the present experiment. The intensity of turbulence of the test section is about 0.1 %, and the thickness of the wall boundary layer at the place where the model was set is of the order of 10 cm.

The model was a light, hollow, foam-plastic rectangular block of a side ratio 2 : 1 having dimensions of 30 cm in length, 15 cm in width and 77 cm in height. Photo 1 shows the model which was set in the second of the test sections mentioned above, whereas the model supporting system is diagrammatically shown in Fig 1. The model was thus mounted on a moving table which was supported by four strips of thin steel plate and was allowed to move perpendicularly to the flow direction in a horizontal plane.

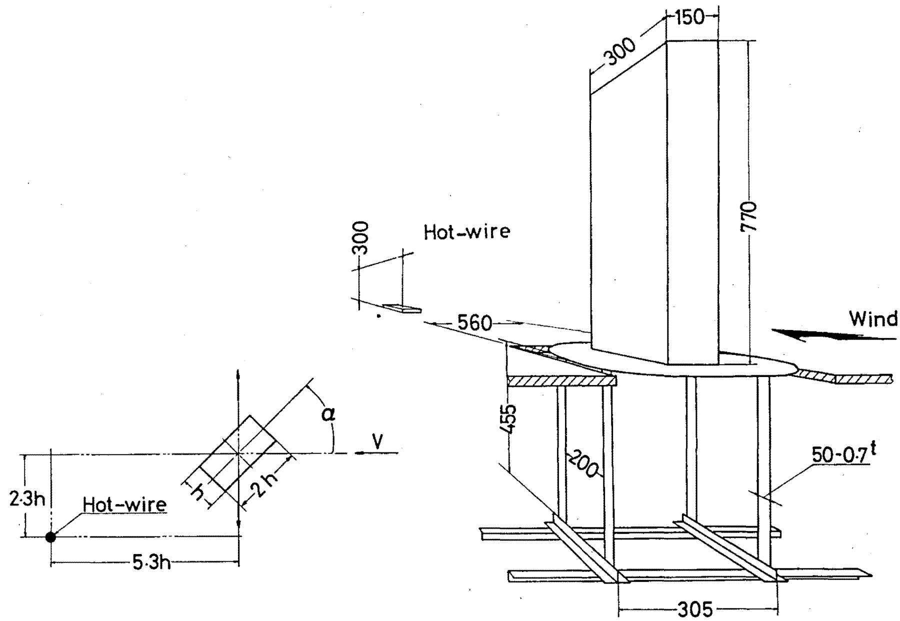

Fig. 1 Illustration of model supporting system and hot-wire probe

The mean angle of attack of the model was varied by loosening the screw nuts which fixed the model with the moving table. Thus, the model was to oscillate perpendicularly to the flow direction for any mean angle of attack. The experiment was made for a range of mean angle of attack from zero deg, i. e., with the shorter side normal to flow direction, to 90 deg, with the longer side normal to the flow direction.

The still-air frequency of the model oscillation was controlled by applying appropriate weights or additional coil springs to the moving table. The model was installed in the test section through a hole opened on the bottom floor. To minimize the effects of the air flow through the hole on the model oscillation, a circular disk of 56 cm in diameter and 2 cm in thickness was fitted on the bottom of the model, the gap between this disk and the bottom floor was about 1.5 cm.

The transverse displacement of the model was measured with the electric wire-strain gauges cemented on the above-mentioned metal strips and was recorded on a direct-reading electromagnetic oscillograph. The time history of the model transverse displacement thus recorded had yielded the non-dimensional limit-cycle amplitude, η_L, and the aerodynamic damping coefficient k_a of the unsteady lift force at some prescribed value of the model amplitude, η, respectively. The linearity of the overall transverse rigidity of the system was good for $\eta \leq 0.5$, approximately; for $\eta > 0.5$, approximately, the system exhibited a hard spring characteristic. For this reason, the measurement of the limit-cycle amplitude for $\eta_L > 0.5$ was not precise, though some of these values of η_L are plotted in the subsequent figures.

The variation of the wake flow velocity during the model oscillation was also monitored by setting up a hot-wire probe at some point behind the model, the location being shown in Fig. 1. The range of the experimental wind speed was from 0.5 to 10 m/sec, approximately, the corresponding range of the Reynolds number based on the shorter side length being 5×10^3 to 1×10^5, approximately.

3. Experimental Results and Discussions

Before showing the results of measurement of this experiment, data for the static aerodynamic force coefficients obtained in a separate experiment[3] are summarized in Fig. 2, where C_L, C_D and C_M respectively denote the aerodynamic lift, drag and moment coefficient. It is shown from Fig. 2 that

$$C_{L\alpha} + C_D > 0 \quad \text{for} \quad 7.5 < \alpha < 65 \text{ deg},$$

and otherwise,

$$C_{L\alpha} + C_D \leqq 0,$$

for the present model. Therefore, according to the quasi-steady aerodynamic theory, galloping may occur for $0 \leqq \alpha \leqq 7.5$ deg or $65 \leqq \alpha \leqq 90$ deg, and the system may be stable for $7.5 < \alpha < 65$ deg. On the other hand, the vortex excitation is expected to occur in some narrow range of reduced velocity including $\overline{V}_{cr}$; here, $\overline{V}_{cr} (=1/S)$ is the reduced velocity at which the vortex frequency for the model at rest coincides with the still-air frequency of the model transverse oscillation.

An experiment using the first of the test sections mentioned earlier was

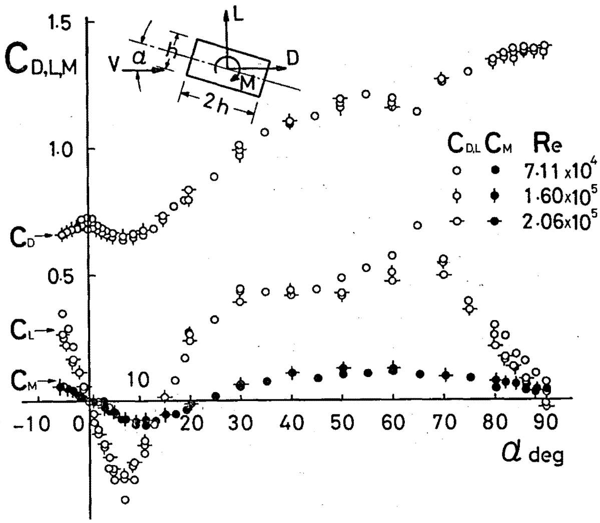

Fig. 2 Static aerodynamic characteristics of the model

carried out for zero mean angle of attack, where the mass and the transverse rigidity of the system were widely varied, the resulting still-air frequency of oscillation being ranged from 0.5 to 4 Hz, approximately.

Fig. 3 shows the variations of the limit-cycle amplitude of oscillation η_L with the reduced velocity $\bar{V}$ for various combinations of the mass ratio and the structural damping. Oscillograms showing representative patterns of the model response together with those of the hot-wire signal are presented in Figs. 4(a) and 4(b). Owing to the large model mass ratio, the frequency of oscillation in the wind differed very little from that in the still air over the whole velocity range tested.

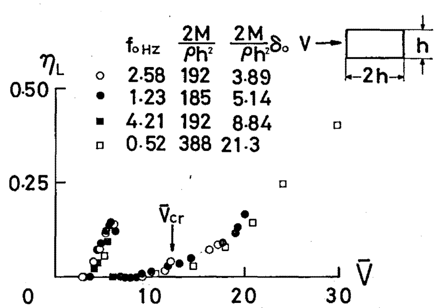

Fig. 3 Limit-cycle amplitude of the model transverse oscillation vs reduced velocity for various combinations of mass and still-air frequency

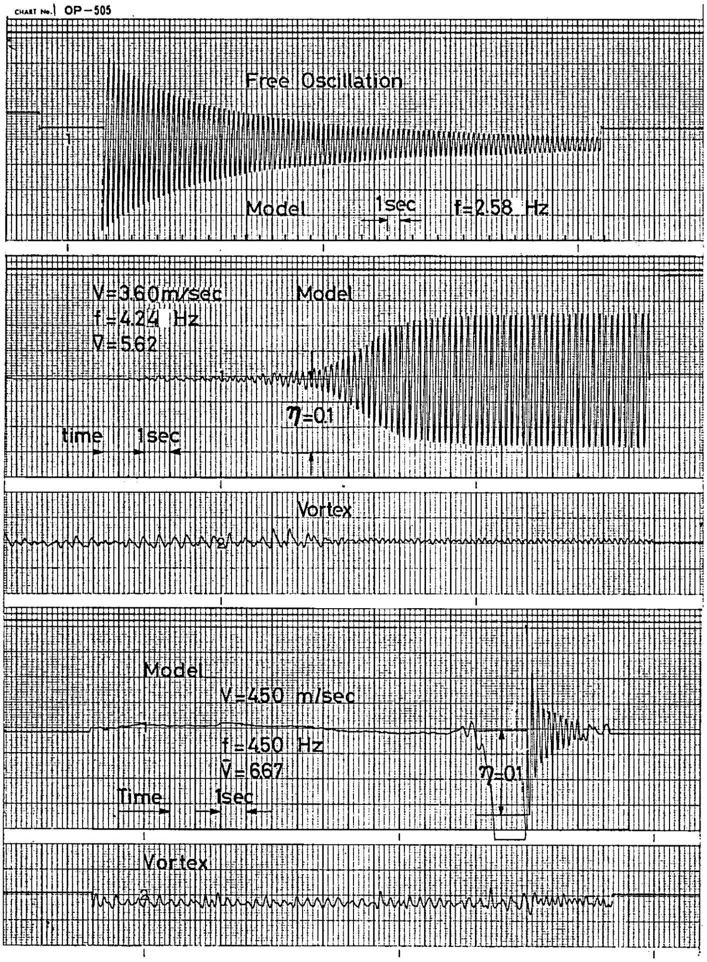

Fig. 4(a)

Figs. 4(a) and 4(b). Typical oscillograms showing the model transverse oscillation and the hot-wire signal

These figures indicate that with an increase in $\overline{V}$, a spontaneous flutter occurred first between $\overline{V}=3.5$ and 6.5, approximately, and then for $\overline{V}>\overline{V}_{cr}$, approximately, with an increasing amplitude. Between the first and the second range of the instability, the oscillation was highly damped. For $\overline{V}>\overline{V}_{cr}$, approximately, the second range of the instability, the limit-cycle amplitude of oscillation was not constant, but the beat modulation of some degree was observed.

By dimensional analysis, η_L is shown to be a function of $\overline{V}$, R and $\frac{2M}{\rho h^2}\,\delta_0$ for a one-degree-of-freedom flutter.[4] Present results indicate good correlation

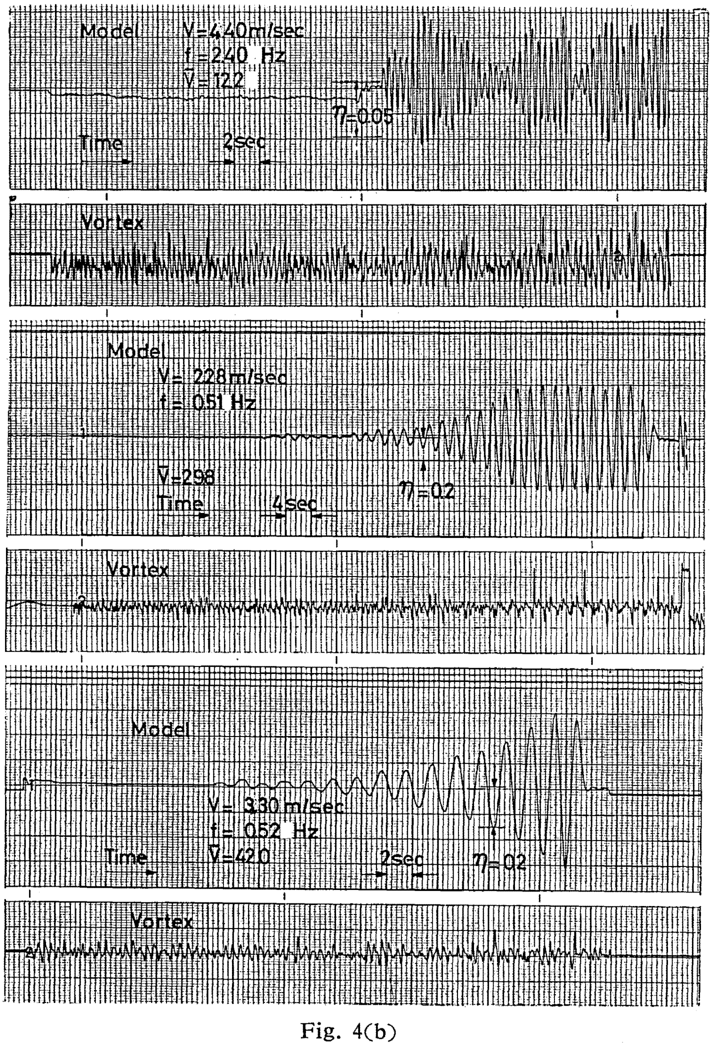

Fig. 4(b)

between η_L and $\bar{V}$ with slight effects of $\frac{2M}{\rho h^2}\delta_0$, as is expected. No serious effects of the Reynolds number on the model response were found at least in the velocity range tested except the fact that the hot-wire signals for the model at rest were less periodic at relatively low wind speeds, i.e., between 0.5 and 2 m/sec, approximately.

The rest of the experiment where the mean angle of attack was varied from zero to 90 deg, was conducted on the model without any additional weights or coil springs applied, utilizing the second of the test sections. No noticeable difference was observed between the results of experiment for $\alpha=0$ deg with the two test sections.

Figs. 5(a) to 5(d) show the η_L vs $\overline{V}$ relationships for representative mean angles of attack. Most of the instabilities occurred spontaneously. In some cases, however, the presence of an unstable limit cycle was known at reduced velocities a little higher than $\overline{V}_{cr}$, namely, the oscillation was damped for $\eta \leq \eta_0$, some critical value, but for $\eta > \eta_0$ it grew up until a stable limit cycle was reached. Fig. 6 presents the stability diagram for the present model together with the curve of $\overline{V}_{cr}$. The figure corresponds to a spontaneous flutter except the area shaded by crossed lines which indicates the existence of an unstable limit cycle. The exact determination of the critical reduced velocity for the second instability was difficult partly because of the gradual increase in amplitude with the reduced velocity and partly because of the beat modulation mentioned earlier.

For mean angles of attack close to zero, the results were essentially similar to that for zero mean angle of attack. The ranges of the reduced velocity for the first and second instabilities remained unchanged. The second instability which started at about $\overline{V} = \overline{V}_{cr}$ for $\alpha = 0$ deg vanished at some value of α between 5 and 7.5 deg, whereas the first instability was present up to some larger value of α, say between 7.5 and 10 deg. The mechanism of the onset of the first

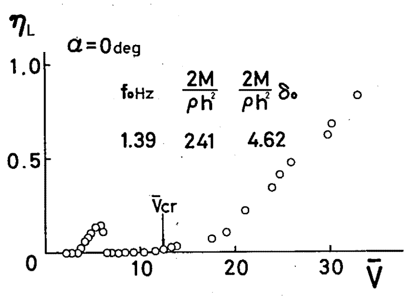

Fig. 5(a)

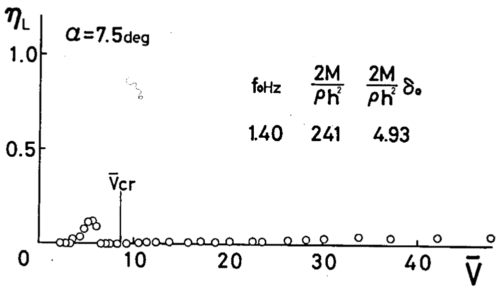

Fig. 5(b)

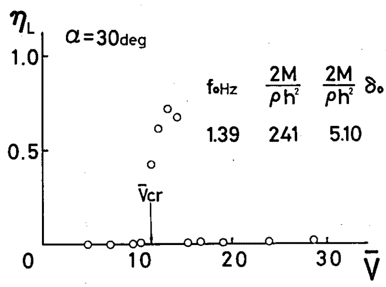

Fig. 5(c)

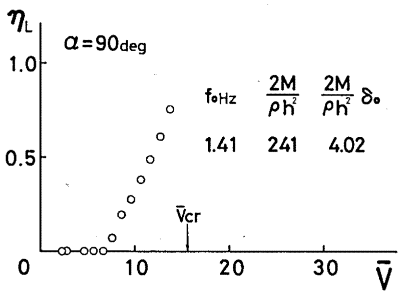

Fig. 5(d)

Figs. 5(a) to 5(d) Limit-cycle amplitude of the model transverse oscillation vs reduced velocity instability is at present unknown, since the correlation between this instability and vortex excitation is not necessarily good as is seen in Fig. 6. The presence of the instability of this type was not reported in Parkinson's paper[2], but was described in a paper by Otsuki and Washizu[5], both of which were concerned with two-dimensional models. Novak also reported the onset of the similar instability for a rectangular block.[6]

For $10<\alpha<30$ deg, approximately, the oscillation was damped for all the reduced velocities tested. For $30<\alpha<65$ deg, approximately, the instability appeared again in a narrow range of $\overline{V}$. This may be attributable to vortex excitation because the range included $\overline{V}_{cr}$, and as will be described later, the aerodynamic excitation took a maximum at $\overline{V}=\overline{V}_{cr}$. A hard flutter characteristic was observed in this range of α at reduced velocities a little higher than $\overline{V}_{cr}$. For $65<\alpha<90$ deg, approximately, the instability started at a reduced velocity well below $\overline{V}_{cr}$, but continued up to the maximum reduced velocity tested. Here again, the aerodynamic excitation took a maximum at $\overline{V}=\overline{V}_{cr}$.

The results presented so far indicate that the instability which was observed at relatively high reduced velocities may be galloping; the sign of the static aerodynamic force coefficient $C_{L\alpha}+C_D$ and the experimental stability boundary are well correlated. This is in agreement with the findings made previously by Parkinson.*) On the other hand, the situation is more complicated at low reduced velocities, where the instability did occur in some restricted ranges of α and $\overline{V}$, but the explanation based on the vortex excitation may not always be successful. It is also worth noting that for $10<\alpha<30$ deg, the periodic vortex street was clearly present for the model at rest, but nevertheless, the vortex excitation did not occur. This fact indicates that the vortex excitation is strongly influenced by the presence of the oscillating afterbody.

In the remaining part, the validity of the quasi-steady aerodynamic theory will be examined more quantitatively. Parkinson[2] had compared the values of the limit-cycle amplitude of oscillation η_L between theory and experiment, whereas in our paper, the aerodynamic damping coefficient k_a of the unsteady lift force will be taken. This is because the comparison of the linear portion between theory and experiment is considered to be more straightforward. Figs. 7 (a) to 7 (d) are the representative examples. Most of the values of k_a in the figures are for $\eta=0.10$, but some values of k_a for $\eta=0.02$ are also plotted in Fig. 7 (a). The theoretical expression for k_a is given by $k_a=(C_{L\alpha}+C_D)\ \overline{V}$.

Before making any comparison between theory and experiment, the follow-

*) The experiment by Parkinson on a two-dimensional model[2] had shown that for $\alpha=90$ deg, the value of $C_{L\alpha}+C_D$ was nearly zero and galloping was not observed, whereas for our present model, the value of $C_{L\alpha}+C_D$ was negative, though quite slightly, and the instability occurred. This difference of our results from Parkinson's is possibly due to the three-dimensional effect of our present model; in particular, our value of C_D which was 1.40 is much smaller than the two-dimensional one which is 2.21.

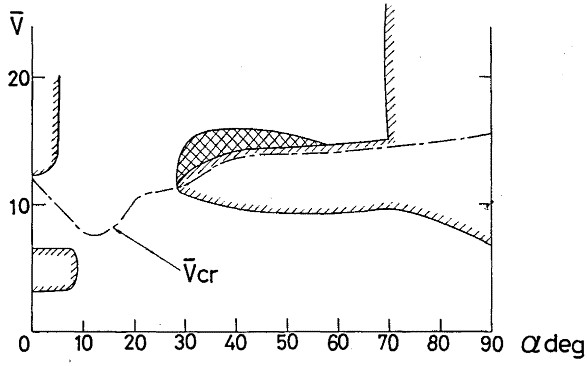

Fig. 6 Diagram showing the stability for the present model

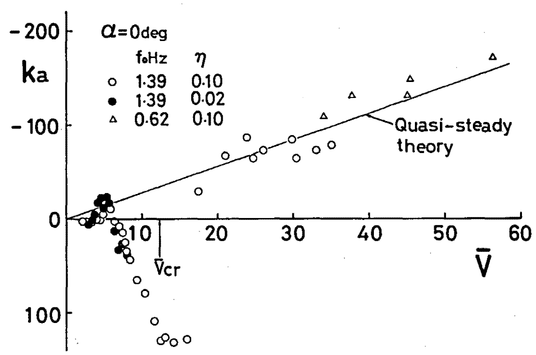

Fig. 7(a)

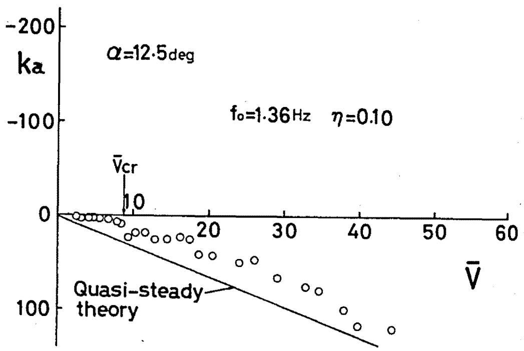

Fig. 7(b)

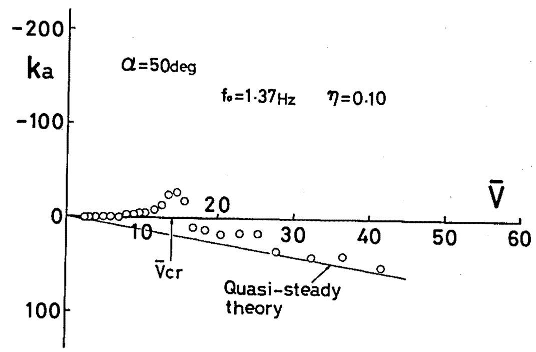

Fig. 7(c)

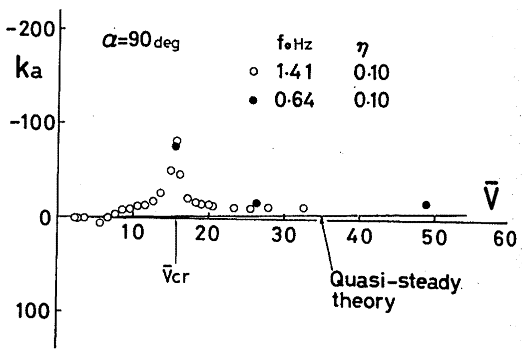

Fig. 7(d)

Figs. 7 (a) to 7 (d) Measured aerodynamic damping coefficients of unsteady lift force ing remark is to be made. At high reduced velocities well over $\overline{V}_{cr}$, the amplitude variations with time in log scale were reasonably approximated by straight lines at least for $\eta \leqq 0.10$ for any mean angle of attack. However, with a decrease in reduced velocity down to $\overline{V}_{cr}$, the effect of the amplitude on k_a was observed in some cases. This effect was most marked at $\overline{V} \cong \overline{V}_{cr}$ for $\alpha=0$ deg, but for α larger than, say, 10 deg, it was negligibly small. There is another lower limit of the reduced velocity involved which depends on the reference amplitude η at which k_a was obtained. This comes from the nonlinearity of the static lift curve. Assuming that the experimental lift curve was linear up to $\alpha=7.5$ deg ($=0.13$ rad) and using the relation, $\dfrac{\dot{y}}{V}=\dfrac{2\pi}{\overline{V}}\eta=0.13$, we get $\overline{V}=4.8$ as an approximate value of the lower limit in the present case, i.e., for $\eta=0.10$.

The experimental values of k_a at high reduced velocities for all the mean angle of attack are shown in fair agreement with the quasi-steady aerodynamic theory. Whether or not the flow unsteadiness is responsible for the remaining discrepancies between theory and experiment at high reduced velocities is at present uncertain, and needs further investigation.

It appears from the figures that the measured values of k_a deviate considerably from the quasi-steady aerodynamic theory when $\overline{V}$ becomes close to $\overline{V}_{cr}$. The variations of k_a at reduced velocities close to $\overline{V}_{cr}$ indicate the presence of large effects of the wake vortices on the model excitation, which are quite dependent on the mean angle of attack. The critical values of $\overline{V}$ at which k_a deviates from the quasi-steady aerodynamic theory is difficult to determine precisely, but a rough estimate for this may be $\overline{V}=2\overline{V}_{cr}$. For $\alpha=90$ deg, the aerodynamic excitation took a maximum at $\overline{V}=\overline{V}_{cr}$, as is shown in Fig. 7 (d). This is the same with $\alpha=50$ deg, but the excitation was much smaller. With further decrease in α, the effects of the wake vortices on k_a seem to be reversed. For $\alpha=0$ deg, the value of k_a changes sign from negative to positive with a decrease in reduced velocity and takes a maximum at $\overline{V} \cong \overline{V}_{cr}$. It is also clear from Fig. 7 (a) that the sign of k_a is again negative between $\overline{V}=3.5$ and 6.5, approximately, i.e., in the range of the first instability.

4. Concluding Remarks

Galloping and vortex excitation were experimentally investigated in a wind tunnel on a rectangular block of a side ratio 2: 1 which was free to oscillate transversely in a uniform flow, where the mean angle of attack was varied from zero to 90 deg. The limit-cycle amplitude of model oscillation and the aerodyamic damping coefficient of unsteady lift force were obtained by a free oscillation technique. The following conclusions may be drawn from the present experiment.

1. The determination of the range of incidence where galloping may occur at high reduced velocities can be made by applying the quasi-steady aerodynamic theory, i.e., by knowing the sign of $C_{L\alpha}+C_D$.

2. The quasi-steady aerodynamic theory gave a rough estimate for the aerodynamic damping coefficient of unsteady lift force at reduced velocities as low as $\bar{V}=2\bar{V}_{cr}$, approximately, for mean angles of attack from zero to 90 deg in the present experiment.
3. The effects of the oscillating afterbody on the vortex excitation are large. In some cases, the periodic vortex street was definitely present for the model at rest, but nevertheless, the oscillation was damped at velocities near $\bar{V}_{cr}$.
4. For mean angles of attack close to zero, an instability took place at reduced velocities well below $\bar{V}_{cr}$, the mechanism of the onset of which is not known at present.

Acknowledgements

The authors are grateful to Mr. M. Tsuuzan and Miss T. Sawai who cordially assisted them in conducting the present investigation. Mr. N. Fukamachi and Mr. K. Watanabe were responsible for the tunnel operation. Mr S. Kaku and Mr. Y. Machida, who have now left the laboratory, also assisted the authors in the early stage of the experiment. Their helps are also acknowledged.

References

1) Den Hartog, J. P., *Mechanical Vibrations*, McGraw-Hill Book Company, Inc., New York, N. Y., fourth edition, 1956, p. 299.
2) Parkinson, G. V., Aeroelastic Galloping in One Degree of Freedom, Proceedings of the conference on Wind Effects on Buildings and Structures held at the NPL, England in June 1963, Vol. II, Her Majesty's Stationery Office, 1965, p. 582.
3) Nakamura, Y. and Mizota, T., Flow Patterns and Aerodynamic Characteristics of a Stationary Rectangular Block, to be published.
4) Scruton, C., On the Wind-excited Oscillations of Stacks, Towers and Masts, Proceedings of the conference on Wind Effects on Buildings and Structures held at the NPL, England in June 1963, Vol. II, Her Majesty's Stationery Office, 1965, p. 798.
5) Otsuki, Y., Washizu, K., Tomizawa, H., Ohya, A. and Fujii, K., Experiments on the Aeroelastic Instability of Prismatic Bars with Rectangular Sections, Preprints of the 3rd conference on Wind Effects on Buildings and Structured held at Tokyo, Japan, September, 1971.
6) Novak, M., Galloping and Vortex Induced Oscillations of Structures, Preprints of the 3rd conference on Wind Effects on Buildings and Structures held at Tokyo, Japan, September, 1971.

(Received September 29. 1971)